Summarizing Coronal Spectra

Vinay Kashyap (SAO), Hyunsook Lee (SAO), Owen Westbrook (SAO)

S.Wolk (SAO), N.Evans (SAO), J.Nichols (SAO), P.Mendrygal (UMinn), J.Slavin (SAO), W.Waldron (EurekaSci)

High-resolution grating spectra of coronal sources contain a tremendous amount of information on the temperature structure and composition of the sources. In general, it requires a painstaking and detailed Emission Measure analysis to extract these parameters from the data. Here, we explore the possibility of summarizing this information in some easily measurable quantities. This is akin to the role played by hardness ratios for low-resolution spectra. Specifically, we measure the ratios of line fluxes in various temperature-, density-, and composition-sensitive lines and compare them to each other and to the underlying continuum. We use as a first test the database of all MEG spectra of cool stars obtained with Chandra to date, and made available via XAtlas (Westbrook et al., 2007). We search for patterns in this high-dimensional space of metrics and report on our capability to group sources according to the measured metrics.
We apply a wavelet-based multi-scale line-detection algorithm to the spectra to identify the locations of lines and to estimate the underlying continuum emission. We then compute various line and continuum ratios (see **Table 1**), and combine them with selected external information (such as $B-V$, the object type, etc) in a multi-way table. We subject subsets of these data to Principal Components Analysis (PCA) and obtain dendrograms to group the stars in different clusters in order to check for trends in the data. The dendrograms are used to obtain subclusters of stars which are again subjected to PCA.
This work is carried out as part of the XAtlas project.

Table 1. Metrics derived from high-resolution spectra

Metric	Flux ratio	Comment
NE2O	Ne X λ12.13 / O VIII λ18.97	tracks Ne abundance
OIF	O VII(i) λ21.8 / O VII(f) λ22.1	O VII is density sensitive
O78	O VII(r) λ21.6 / O VIII λ18.97	tracks temperature
O2FE	O VIII λ18.97 / Fe XVII $\lambda\lambda$15.01,17.1	tracks low FIP element abundances
MG2FE	Mg XIIλ8.419 / Fe XVII $\lambda\lambda$15.01,17.1	high FIP element, tracks fractionation
SI2FE	Si XIVλ6.18 / Fe XVII $\lambda\lambda$15.01,17.1	high FIP element, tracks fractionation
S2FE	S XV λ5.1 / Fe XVII $\lambda\lambda$15.01,17.1	intermediate FIP element
SL2C, short line/cont	$f_{\rm line}(\lambda < 12.13)$ / $f_{\rm continuum}$	sensitive to high temperatures and metallicities
LL2C, long line/cont	$f_{\rm line}(\lambda > 12.13)$ / $f_{\rm continuum}$	sensitive to low temperatures
L2C, line/cont	$f_{\rm line}$ / $f_{\rm continuum}$	tracks metallicity
CL2CS, cont long/short	$f_{\rm continuum}(13 < \lambda < 25)$ / $f_{\rm continuum}(3 < \lambda < 12)$	categorizes continuum shape
CL2CM, cont long/medium	$f_{\rm continuum}(13 < \lambda < 25)$ / $f_{\rm continuum}(6 < \lambda < 12)$	categorizes continuum shape
CM2CS, cont medium/short	$f_{\rm continuum}(6 < \lambda < 12)$ / $f_{\rm continuum}(3 < \lambda < 6)$	categorizes continuum shape

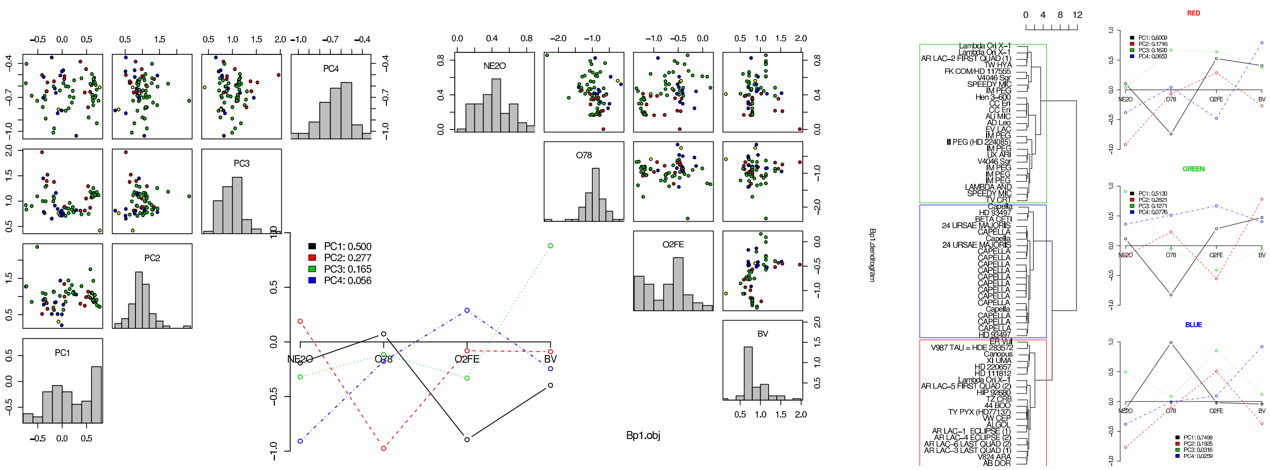

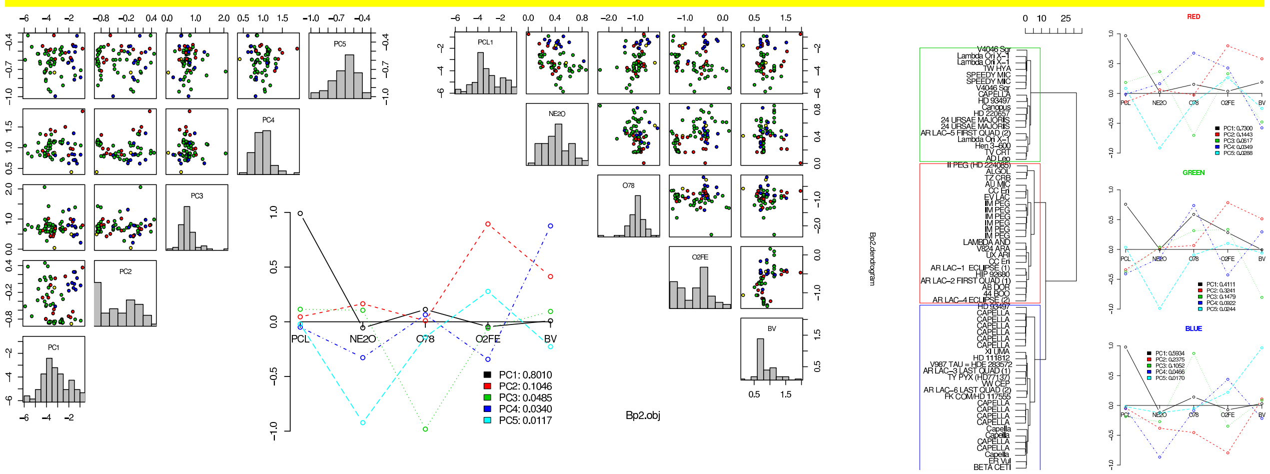

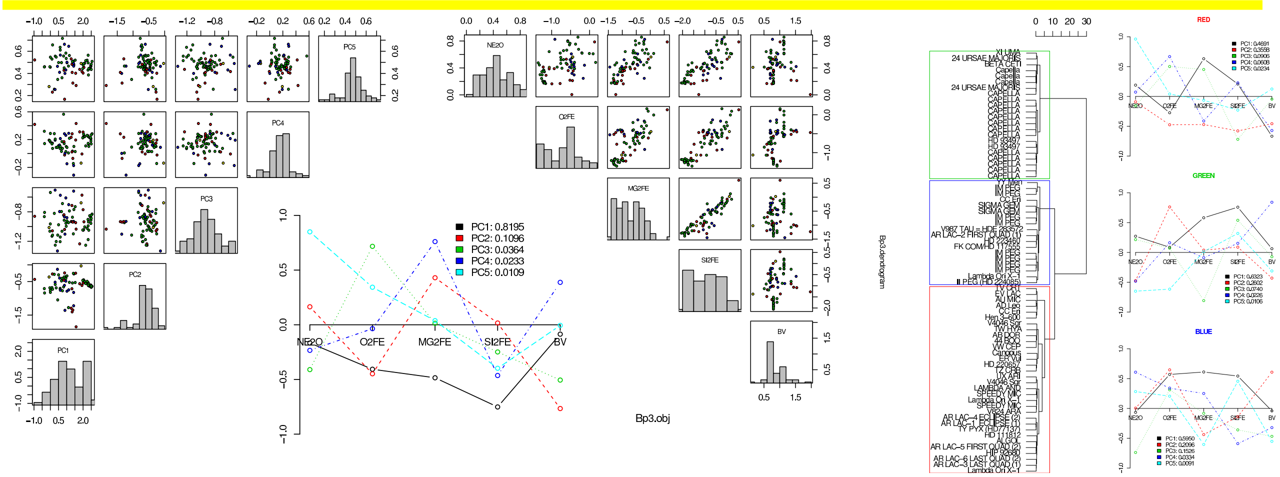

PCA

Principal Component Analysis (PCA) is a method to identify the vectors that describe the scatter of the dataset by approximating the scatter as an ellipsoid. Each vector is a linear combination of the variables that define the dataset. The first component finds the axis of largest scatter, and typically represents the dominant correlation.

Dendrograms

For low-dimensional data, the clustering usually present in data points which have similar variable values is easily visible. But for high-dimensional data, it is difficult to visualize the clustering and determine the number of classes. We perform hierarchical cluster analysis with Euclidean distance in log space for measuring dissimilarity. Hierarchical clustering begins with an individual data point and its nearest neighbors (defined based on various distance measures: Euclidean, maximum, Manhattan L_1, Minkowski, etc.) The closest points are grouped into clusters, and the clusters and other points are then grouped further using similar distance measures. For this, we use the "Ward" method which uses the centroid of a cluster as its defining location. This merging process continues until one cluster is left and is realized by a *Dendrogram*. We carry out additional Principal Component analyses on the subsets that define the 3 largest clusters.

The figures show the results of the PCA (left) and dendrograms (with each leaf labeled with the name of the star) of the cluster analysis and subsequent PCA on the subclusters (right) for three different subsets of flux ratio metrics. The grid plots show scatter plots for each principal component (left grid) and for the original variables (right grid). The weights of the vectors defining each individual principal component is displayed in between the two grid plots.

Case 1

- Ne/O
- O VIIr/O VIII
- O VIII/Fe XVII
- $B-V$

Case 2

- PCA(SL2C,LL2C,L2C,CL2CS,CL2CM)
- rest as in Case 1

Case 3

- Ne/O
- O VIII/Fe XVII
- Mg XII/Fe XVII
- Si XIV/Fe XVII
- $B-V$

CONCLUSIONS

We have carried out an exploratory analysis of the features in spectra of active binaries, T-Tauri stars, and normal single coronal sources obtained with the *Chandra*/HETGS, and find some interesting trends in the dataset:

1: the ratios Ne/O, O7/O8, O/Fe, and $B-V$ are essentially independent

2: the ratios SL2C, LL2C, L2C, CL2CS, CL2CM are tightly correlated (and have been replaced by a single variable PCL, which is the first Principal component from a PCA applied to them)

3: stellar coronal metrics are on average very weakly (if at all) dependent on $B-V$

4: O, Mg, and Si tend to increase or decrease together relative to Fe, but superposed on this is an opposite trend that manifests in some subclusters

5: Multiple observations of the same star are usually found in the same subcluster, providing a post hoc justification for the robustness of the dendrograms

More analysis is needed to robustly identify and extract other trends that appear to exist within the dataset.

This research is supported by Chandra Grants GO5−6006 and GO5−6006A, NASA contract NAS8−39073 to the Chandra X−ray Center, and NASA/AISRP grant NNG06GF17G